

Tomographic Separation of Composite Spectra. X. The Massive Close Binary HD 101131

Douglas R. Gies¹

*Center for High Angular Resolution Astronomy and
Department of Physics and Astronomy,
Georgia State University, Atlanta, GA 30303;
gies@chara.gsu.edu*

Laura R. Penny²

*Department of Physics and Astronomy,
College of Charleston,
Charleston, SC 29424;
pennyl@cofc.edu*

Pavel Mayer

*Astronomical Institute, Charles University,
V Holešovičkách 2, CZ-180 00 Praha 8, Czech Republic;
mayer@cesnet.cz*

Horst Drechsel and Reinald Lorenz

*Dr. Remeis-Sternwarte Bamberg, Astronomisches Institut der Universität
Erlangen-Nürnberg, Sternwartstrasse 7, D-96049 Bamberg, Germany;
drechsel@sternwarte.uni-erlangen.de, lorenz@sternwarte.uni-erlangen.de*

ABSTRACT

We present the first orbital elements for the massive close binary HD 101131, one of the brightest objects in the young open cluster IC 2944. This system is a double-lined spectroscopic binary in an elliptical orbit with a period of

¹Guest Observer, Mount Stromlo and Siding Springs Observatories, Australia

²Guest Observer, Complejo Astronomico El Leoncito (CASLEO), San Juan, Argentina

9.64659 ± 0.00012 days. It is a young system of unevolved stars (approximately 2 million years old) that are well within their critical Roche surfaces. We use a Doppler tomography algorithm to reconstruct the individual component optical spectra, and we apply well known criteria to arrive at classifications of O6.5 V((f)) and O8.5 V for the primary and secondary, respectively. We compare the reconstructed spectra of the components to single-star spectrum standards to determine a flux ratio of $f_2/f_1 = 0.55 \pm 0.08$ in the V -band. Both components are rotating faster than synchronously. We estimate the temperatures and luminosities of the components from the observed spectral classifications, composite V magnitude, and cluster distance modulus. The lower limits on the masses derived from the orbital elements and the lack of eclipses are $25M_\odot$ and $14M_\odot$ for the primary and secondary, respectively. These limits are consistent with the larger masses estimated from the positions of the stars in the Hertzsprung-Russell diagram and evolutionary tracks for single stars.

Subject headings: binaries: spectroscopic — open clusters and associations: individual (IC 2944) — stars: early-type — stars: fundamental parameters — stars: individual (HD 101131)

1. Introduction

The hot star HD 101131 (HIP 56726, LS 2420) is found in the heart of the young open cluster IC 2944. This cluster contains a population of some dozen relatively unevolved O-type stars (Walborn 1987; Mermilliod 1995)³ that form the ionizing source of the surrounding H II region, Gum 42 (Georgelin et al. 2000). The two brightest members of the cluster are HD 101131 (O6 V ((f)); Walborn (1973)) and its nearby companion, HD 101205 (O7 III_n ((f)); Walborn (1973)). HD 101131 appears single in speckle interferometric observations (Mason et al. 1998), but the spectroscopic evidence to date suggests that it is a close, unresolved binary. Feast et al. (1955) were the first to suspect its spectroscopic binary nature, and they observed double-lines on several occasions. Thackeray & Wesselink (1965) reported on new radial velocity measurements and plans to determine the orbit, but, unfortunately, subsequent results were never published. The system has been relatively neglected since, save for a single radial velocity measurement by Conti et al. (1977) and one double-lined

³See also <http://obswww.unige.ch/webda>, a Web site devoted to stellar open clusters created by J.-C. Mermilliod.

observation made with the *International Ultraviolet Explorer Satellite (IUE)* (Penny 1996; Howarth et al. 1997; Stickland & Lloyd 2001).

We have explored the properties of a number of massive binaries in this series of papers using UV spectra available in the *IUE* archive. However, in a recent paper (Penny et al. 2002), we applied many of the same techniques to new optical spectra obtained from the CASLEO and Mount Stromlo Observatories in 1997 and 1998, respectively. HD 101131 was also a target during these runs, and here we present the first orbit for this massive binary. We discuss the observations and radial velocity measurements for this double-lined system in §2. We then apply a version of the Doppler tomography algorithm to reconstruct the individual spectra of both components, from which we determine their spectral classifications, projected rotational velocities, and flux ratio (§3). Finally, we discuss the probable masses and evolutionary state of the binary in §4.

2. Observations and Radial Velocities

Our spectra were obtained mainly in two observing runs at different sites (see Penny et al. (2002) for details). The first set was obtained with the 2.15-m telescope of the Complejo Astronomico El Leoncito (CASLEO) and REOSC echelle spectrograph during the period 1997 March 19 – 28. The detector was a TEK 1024 × 1024 CCD with 24 μm square pixels. We extracted 23 orders from these echellograms, and the resulting spectra span the range from 3575 to 5700 Å with a spectral resolving power of $\lambda/\Delta\lambda = 13,000$ (with a signal-to-noise ratio of ≈ 150 per pixel in the better exposed portions of the spectrum).

Our second observing run took place at the 74-inch telescope at Mount Stromlo Observatory over the period 1998 April 6 – 14. These spectra were made with the coude spectrograph and a SITE CCD detector (D14) with 15 μm square pixels in a 4096 × 2048 format. The resulting single order spectra cover the range 3804 – 4220 Å with a reciprocal dispersion of 0.10 Å per pixel and a resolution element of 0.30 Å FWHM ($\lambda/\Delta\lambda = 13400$ at 4012 Å). The MSO spectra have a typical S/N equal to 160 pixel⁻¹ in the continuum.

The spectra were reduced using standard routines in IRAF⁴. The extracted orders of the CASLEO echellograms were rectified to a unit continuum by fitting a high order spline function to line-free regions. Small amplitude irregularities related to this fitting of the

⁴IRAF is distributed by the National Optical Astronomy Observatories, which is operated by the Association of Universities for Research in Astronomy, Inc., under cooperative agreement with the National Science Foundation.

echelle blaze function were evident in the continuum, and the same pattern was seen in all spectra made on a given night. We were able to remove most of the pattern by dividing the target spectrum by a correction spectrum formed from spectra of B-star, τ Sco, which was also observed each night. The correction spectrum was a smoothed version of the particular night's τ Sco spectrum divided by a global average representation of this star's stellar spectrum. The spectra from each run were collected and transformed onto their respective heliocentric wavelength grids.

A visual inspection of the spectra immediately showed evidence of cyclic variation in profile shape over a period of approximately 10 days. However, the binary components were only cleanly separated in the He I $\lambda\lambda 4026, 4471$ profiles of spectra obtained near the orbital quadrature phases. Thus, we decided to measure these generally blended features using a scheme of fitting single-star template spectral lines to our observed composite spectra (Penny et al. 2002).

We used the star HD 57682 (O9 IV; Walborn (1972)), which was observed in both runs, as the template for the fainter secondary, but, unfortunately, we observed no hot star in common between the CASLEO and MSO runs that could be used as a template for the primary. We selected HD 93160 (O6 III(f); Walborn (1972)) as the primary star template for the CASLEO spectra, and we used HD 164492 (O7 III((f)); Walborn (1972)) as the template for the MSO spectra. All of the template spectra stars appeared to be constant-velocity objects in our observations. The individual spectra for each template were averaged together to improve the signal-to-noise ratio (S/N), shifted to the rest frame, and any obvious interstellar lines were excised. The radial velocities of the template stars were measured by parabolic fitting of lines taken from the list of Bolton & Rogers (1978), and we found average radial velocities of $+25.0 \pm 0.5$ and $+26.0 \pm 1.1$ km s⁻¹ from the CASLEO and MSO spectra, respectively, for HD 57682; -1.0 ± 2.3 km s⁻¹ for HD 93160 (CASLEO); and $+5.3 \pm 0.9$ km s⁻¹ for HD 164492 (MSO).

Next, we artificially broadened each template spectrum by convolution with a rotational broadening function to produce profiles that matched the spectral components of HD 101131 in the best-separated quadrature spectra. We also used these resolved profiles to estimate the line-depth ratio between the components. Once these fitting parameters were set, we determined the radial velocities of each component for a given line by a least-squares fit of the observed profile with the co-addition of the two template profiles shifted in wavelength to obtain the best match. We used this technique to measure radial velocities for the strongest lines in the CASLEO spectra, specifically H I $\lambda\lambda 3797, 3835, 3889, 3970, 4101, 4340, 4861$; He I $\lambda\lambda 4026, 4471, 4713, 5015$; He II $\lambda\lambda 4199, 4541, 5411$; and O III $\lambda 5592$. A subset of these (plus the C III $\lambda 4070$ blend) was measured in the smaller wavelength range of the MSO

spectra.

There was no evidence of systematic line-to-line differences in the radial velocity measurements, and so no line-specific corrections were applied. The radial velocities from all the available lines were averaged together after deletion of any very discrepant measurements. Finally, we made small adjustments to these averages based on measurements of the strong interstellar Ca II $\lambda\lambda 3933, 3968$ lines. An interstellar spectrum was formed by extracting the mean spectrum in the immediate vicinity of each interstellar absorption line. (We made Gaussian fits of the interstellar Ca II profiles in the average spectra, and we found the radial velocity was -6.4 ± 0.2 and -4.9 ± 0.3 km s $^{-1}$ for the CASLEO and MSO spectra, respectively.) We then cross correlated this spectrum with each individual spectrum to measure any small deviations in our wavelength calibration (generally < 2 km s $^{-1}$), and these small corrections were applied to the mean velocities. Table 1 lists the heliocentric dates of mid-observation, orbital phase, and, for each component, the mean radial velocity, the standard deviation of the mean, the observed minus calculated ($O - C$) residual from the orbital fit, and the number of lines used in the mean.

We also obtained 8 high resolution CCD spectra between 1992 and 1994 using the European Southern Observatory (ESO) 1.52-m telescope, equipped with the ECHELEC echelle spectrograph, and the ESO 1.4-m coudé auxiliary telescope feeding the coudé echelle spectrograph of the ESO 3.6-m telescope (Lorenz et al. 1999). Radial velocities measured from these spectra are listed in Table 1 along with data from Feast et al. (1955), Conti et al. (1977), and Stickland & Lloyd (2001). After publishing the radial velocities of HD 101131 in 1955, the Radcliffe Observatory staff obtained more spectra. These were made available to one of us (PM); due to the low dispersion of these plates and the wide spectral lines, only the primary component (or the blended feature) was visible. We measured radial velocities by matching the line profile with its wavelength reversed version (Lorenz et al. 1999). Usually only H γ and H δ were measurable, but in some cases results for several He I lines were included in forming the mean radial velocity (listed in Table 1).

We made a preliminary period search using a version of the discrete Fourier transform and CLEAN deconvolution algorithm of Roberts et al. (1987) (written in IDL⁵ by A. W. Fullerton), and the position of the strongest peak in the CLEANed power spectrum for the primary velocities was used as the starting value for a general solution of the orbital elements using the nonlinear, least-squares fitting program of Morbey & Brosterhus (1974). We found that the scatter in the pre-1995 measurements was significantly larger than in CASLEO and MSO results and that these early data were often affected by pair blending with the

⁵IDL is a registered trademark of Research Systems, Inc.

secondary’s lines, so we made a final fit by assigning a lower weight (0.10) to the earlier data. The secondary radial velocity measurements have larger associated errors, so we fitted these for the systemic velocity, V_0 , and semi-amplitude, K , only with the other elements set by the solution for the primary. The solutions are listed in Table 2, and the combined radial velocity curve is illustrated in Figure 1.

We find residuals from the fit that are approximately 18% of the projected rotational velocities (§3), which is not unexpected given the severe line blending in most of the spectra. The system apparently has a significant eccentricity, but this is not unusual for binaries with similar periods (Mason et al. 1998). The systemic velocities of the two components are approximately 3σ apart. The primary’s systemic velocity is more negative than the secondary’s value, which is what we would expect due to line formation in the greater outflow from photosphere to wind in the more luminous primary. Thackeray & Wesselink (1965) find a mean radial velocity of $+1.1 \text{ km s}^{-1}$ for the bright, hot stars in IC 2944, a value which sits comfortably between our results for the systemic velocities and which is probably close to the physical systemic velocity of the binary.

3. Tomographic Reconstruction

We used the Doppler tomography algorithm described by Bagnuolo et al. (1994) to reconstruct the individual primary and secondary spectra independently from the CASLEO and MSO spectra. We took the radial velocity shifts for each component from the orbital solutions in Table 2, then the reconstruction was run for 50 iterations with a gain of 0.8 (the results are insensitive to both parameters). The reconstructed spectra are plotted in in Figure 2 in a format similar to that used in the spectral atlas of Walborn & Fitzpatrick (1990). The reconstructions from the MSO spectra are shown just above those from the CASLEO spectra (in the short wavelength portion of Fig. 2), and there is good agreement between these two sets of spectra.

We compared the reconstructed spectra with the spectrum standards in the atlas of Walborn & Fitzpatrick (1990) to determine the spectral classifications of the components. The strengths of the He I $\lambda\lambda 4026, 4471$ lines relative to those of He II $\lambda\lambda 4200, 4541$ are all consistent with a spectral type of O6.5 for the primary. In particular, the weak but convincing presence of He I $\lambda 4387$ is more consistent with the O6.5 type than the O6 V((f)) type given for the composite spectrum by Walborn (1973). The small ratio of Si IV $\lambda 4088$ to He I $\lambda 4026$ indicates a main sequence class, as does the near equality of He II $\lambda 4686$ and He II $\lambda 4541$. Thus, we classify the primary as type O6.5 V((f)), where the suffix indicates the presence of weak emission in N III $\lambda\lambda 4634 - 4640 - 4642$. We compare its spectrum in

Figure 2 to that of HD 93146, which is given as the standard of this class in Walborn & Fitzpatrick (1990).

The secondary, on the other hand, has features indicating a cooler temperature and later type. All the He I transitions appear stronger in the secondary’s spectrum, and the defining ratios of He II $\lambda 4541$ /He I $\lambda 4387$ and He II $\lambda 4200$ /He I $\lambda 4144$ are most consistent with a type of O8.5. The relative strength of the Si IV $\lambda\lambda 4088, 4116$ lines compared to the neighboring He I $\lambda\lambda 4121, 4144$ features indicates a luminosity class V, as does the robust strength of He II $\lambda 4686$. Figure 2 illustrates the good agreement between the spectrum of the secondary and that of HD 46149, which Walborn & Fitzpatrick (1990) use as a standard for type O8.5 V.

The two spectral standards, HD 93146 and HD 46149, provided us with the means to estimate the visual flux ratio, $r = F_2/F_1$, by matching the line depths in the reconstructed spectra with those in the standards. This was done by aligning the reconstructed and standard spectra, adjusting for differences in the placement of the continuum, Gaussian smoothing of the spectra to eliminate differences in projected rotational velocity and instrumental broadening, and then finding a best-fitted line ratio that allocates a proportion of flux to each component to best match the line depths. We found $r = 0.52 \pm 0.12$ and 0.56 ± 0.12 for the MSO and CASLEO reconstructions, respectively, and we adopted the mean result, $r = 0.54 \pm 0.08$, for the depictions of the reconstructed spectra in Figure 2.

Finally, we used the reconstructed spectra to estimate the projected rotational velocities of the components. Our procedure involved calculating a grid of rotational broadening functions for a linear limb darkening law (Wade & Rucinski 1985; Gray 1992) and then convolving an observed narrow-lined spectrum with these broadening functions. We focused on the Si IV $\lambda 4088$ profile for the primary’s spectrum since it represents the strongest metallic line (intrinsically narrow) in the range covered by the MSO spectra. We compared the spectral reconstructions from the CASLEO and MSO spectra with broadened versions of the spectrum of the narrow-lined star HD 164492 ($V \sin i = 48 \text{ km s}^{-1}$, Penny (1996)). The best fitting profile matches with the primary’s spectrum were made with $V \sin i = 102 \pm 10 \text{ km s}^{-1}$. The secondary’s spectrum shows stronger He I features in the MSO range, so we fit all the profiles in the range between He I $\lambda 4009$ and Si IV $\lambda 4088$. Here we compared the secondary’s spectrum with broadened versions of the spectrum of the star HD 57682 ($V \sin i = 33 \text{ km s}^{-1}$, Penny (1996)), and the best fits were made with $V \sin i = 164 \pm 12 \text{ km s}^{-1}$. These are comparable to the estimates from the *IUE* observation (Penny 1996; Howarth et al. 1997; Stickland & Lloyd 2001).

4. Discussion

The mass limits derived from the orbit, $M \sin^3 i$ (Table 2), are quite large, and given the relative scarcity of data on the masses of O-type stars (Burkholder et al. 1997), it is important to compare our results with predictions based on evolutionary tracks. Since HD 101131 is a member of the cluster IC 2944, we can use the cluster distance modulus to help place the individual component stars in the H-R diagram. We estimated the stellar temperatures from the spectral classifications using the calibrated sequence given by Howarth & Prinja (1989). These temperatures and other stellar parameters are listed in Table 3. We used flux models from Kurucz (1994) to transform our observed flux ratio based upon the relative line depths in the blue part of the spectrum into a V -band flux ratio (Penny et al. 1997), $f_2(V)/f_1(V) = 0.55 \pm 0.08$, so that we could determine the V magnitude of both components. We adopted the composite magnitude, $V = 7.16$, and cluster distance modulus, $m - M = 12.5 \pm 0.2$, from Thackeray & Wesselink (1965), which agree well with more recent estimates (Tovmassian et al. 1998). We used the bolometric corrections given by Howarth & Prinja (1989) to arrive at estimates of the individual luminosities, and these are listed in Table 3. Table 3 also includes the resulting stellar radii estimates. We calculated the sizes of the Roche volume radius (Eggleton 1983) of both stars for the time of smallest separation (Table 3), and both are well within their critical Roche surfaces then, even after accounting for their rapid rotation (Limber 1963). Thus, given these stellar dimensions and the youthful appearance of the IC 2944 cluster, it is safe to assume that the interacting stage in this system lies far in the future and that we can compare the stars' evolutionary state with the predictions for single stars with the same physical parameters.

The primary and secondary components are placed in the H-R diagram in Figure 3 together with the evolutionary tracks for single stars from the models of Schaller et al. (1992). Both stars appear close to the zero-age main sequence, and an interpolation in these tracks gives ages of 1.5 ± 0.4 and 2.7 ± 0.8 million years for the primary and secondary, respectively. The predicted current masses from these evolutionary tracks are listed in Table 3. Note that both stars are relatively rapid rotators (with angular velocities greater than 2 and 4 times synchronous for the primary and secondary, respectively). Rapidly rotating stars may have luminosities larger than their nonrotating counterparts (Heger & Langer 2000; Meynet & Maeder 2000), so the predicted masses given in Table 2 may be slight overestimates.

Lower limits for the masses can be taken directly from the $M \sin^3 i$ values, but we can improve these somewhat from light-curve considerations. The target was observed by the *Hipparcos* satellite (Perryman 1997), and we examined the *Hipparcos* epoch photometry data for any evidence of eclipses based on our orbital ephemeris. There is no sign of any eclipse deeper than 0.01 mag, so we can use the lack of eclipses together with our estimates of the

binary separation at superior conjunction of the primary (the closer of the two conjunctions) and the stellar radii to find an upper limit on the orbital inclination, $i < (72^{\circ}0 \pm 1^{\circ}6)$. The resulting lower limits for the stellar masses are listed in the final row of Table 3. We find that the predicted masses are somewhat larger than these lower limits, and, in fact, if the evolutionary masses are correct, then the system inclination is actually $i = 56^{\circ} \pm 2^{\circ}$. A second consistency check is obtained from the implied mass ratio from the evolutionary models, $q = M_2/M_1 = 0.63 \pm 0.05$, that agrees within errors with the observed mass ratio, $q = 0.56 \pm 0.02$. Thus, we find that the constraints on the system masses provided by the orbital elements and distance modulus are fully consistent with the predictions from evolutionary tracks, in agreement with the conclusions of Burkholder et al. (1997) for other unevolved close binary systems. The predicted maximum angular separation is 0.15 mas, which may be within the reach of future optical interferometers.

We thank the staffs of CASLEO and MSO for their assistance in making these observations. We also thank Alex Fullerton for sharing his period search code with us. We are grateful to Dr. T. Lloyd Evans (SAAO), who kindly arranged the plate loan, and to Mr. J. Havelka (Astronomical Institute, Czech Academy of Sciences) who digitized these plates. Institutional support for L.R.P. has been provided from the College of Charleston School of Sciences and Mathematics. Additional support for L.R.P. was provided by the South Carolina NASA Space Grant Program and NSF grant AST-9528506. Institutional support for D.R.G. has been provided from the GSU College of Arts and Sciences and from the Research Program Enhancement fund of the Board of Regents of the University System of Georgia, administered through the GSU Office of the Vice President for Research. We gratefully acknowledge all this support.

REFERENCES

- Bagnuolo, W. G., Jr., Gies, D. R., Hahula, M. E., Wiemker, R., & Wiggs, M. S. 1994, *ApJ*, 423, 446
- Bolton, C. T., & Rogers, G. L. 1978, *ApJ*, 222, 234
- Burkholder, V, Massey, P., & Morrell, N. 1997, *ApJ*, 490, 328
- Conti, P. S., Leep, E. M., & Lorre J. J. 1977, *ApJ*, 214, 759
- Eggleton, P. P. 1983, *ApJ*, 268, 368
- Feast, M. W., Thackeray A. D., & Wesselink, A. J. 1955, *Mem. Roy. Astron. Soc.*, 67, 51
- Georgelin, Y. M., Russeil, D., Amram, P., Georgelin, Y. P., Marcelin, M., Parker, Q. A., & Viale, A. 2000, *A&A*, 357, 308
- Gray, D. F. 1992, *The Observation and Analysis of Stellar Photospheres* (2nd ed.) (Cambridge: Cambridge Univ. Press)
- Heger, A., & Langer, N. 2000, *ApJ*, 544, 1016
- Howarth, I. D., & Prinja, R. K. 1989, *ApJS*, 69, 527
- Howarth, I. D., Siebert, K. W., Hussain, G. A. J., & Prinja, R. K. 1997, *MNRAS*, 284, 265
- Kurucz, R. L. 1994, *Solar Abundance Model Atmospheres for 0, 1, 2, 4, 8 km/s*, Kurucz CD-ROM No. 19 (Cambridge, MA: Smithsonian Astrophysical Obs.)
- Limber, D. N. 1963, *ApJ*, 138, 1112
- Lorenz, R., Mayer, P., & Drechsel, H. 1999, *A&A*, 345, 531
- Mason, B. D., Gies, D. R., Hartkopf, W. I., Bagnuolo, W. G., Jr., ten Brummelaar, T., & McAlister, H. A. 1998, *AJ*, 115, 821
- Mermilliod J.-C. 1995, in *The Origins, Evolution, and Destinies of Binary Stars in Clusters* (A.S.P. Conf. Ser. Vol. 90), ed. E. F. Milone & J.-C. Mermilliod (San Francisco: A.S.P.), 475
- Meynet, G., & Maeder, A. 2000, *A&A*, 361, 101
- Morbey, C. L., & Brosterhus, E. B. 1974, *PASP*, 86, 455

- Penny, L. R. 1996, *ApJ*, 463, 737
- Penny, L. R., Gies, D. R., & Bagnuolo, W. G., Jr. 1997, *ApJ*, 483, 439
- Penny, L. R., Gies, D. R., Wise, J. H., Stickland, D. J., & Lloyd, C. 2002, *ApJ*, 575, August 20 issue, in press
- Perryman, M. A. C. 1997, *The Hipparcos and Tycho Catalogues*, ESA SP-1200 (ESA/ESTEC, Noordwijk)
- Roberts, D. H., Lehár, J., & Dreher, J. W. 1987, *AJ*, 93, 968
- Schaller, G., Schaerer, D., Meynet, G., & Maeder, A. 1992, *A&AS*, 96, 269
- Stickland, D. J., & Lloyd, C. 2001, *Observatory*, 121, 1
- Thackeray, A. D., & Wesselink, A. J. 1965, *MNRAS*, 131, 121
- Tovmassian, H. M., Epremian, R. A., Hovhannessian, Kh., Cruz-Gonzalez, G., Navarro, S. G., & Karapetian, A. A. 1998, *AJ*, 115, 1083
- Wade, R. A., & Rucinski, S. M. 1985, *A&AS*, 60, 471
- Walborn, N. R. 1972, *AJ*, 77, 312
- Walborn, N. R. 1973, *AJ*, 78, 1067
- Walborn, N. R. 1987, *AJ*, 93, 868
- Walborn, N. R., & Fitzpatrick, E. L. 1990, *PASP*, 102, 379

Table 1. Radial Velocity Measurements

HJD (-2,400,000)	Orbital Phase	V_1 (km s ⁻¹)	σ_1 (km s ⁻¹)	$(O - C)_1$ (km s ⁻¹)	n_1	V_2 (km s ⁻¹)	σ_2 (km s ⁻¹)	$(O - C)_2$ (km s ⁻¹)	n_2
34060.492 ^a ..	0.570	106.0	...	29.9	6	-155.0	...	-20.4	3
34086.394 ..	0.255	-60.0	...	27.6
34094.377 ^a ..	0.083	-121.0	...	5.1	6	206.0	...	-23.6	2
34107.349 ^a ..	0.427	27.0	...	16.0	5
34114.380 ^a ..	0.156	-134.0	...	-6.3	3
34144.298 ^a ..	0.258	-117.0	...	-30.8	7	153.0	...	-4.8	2
34179.210 ^a ..	0.877	-25.0	...	-62.9	6
34193.192 ^a ..	0.326	-12.0	...	35.0	7
34768.580 ..	0.973	16.0	...	67.9
35594.308 ..	0.571	128.0	...	51.6
36595.565 ..	0.365	-34.0	...	-9.6
36598.533 ..	0.673	56.0	...	-44.6
36599.472 ..	0.770	37.0	...	-57.4
36602.499 ..	0.084	-104.0	...	22.3
36604.493 ..	0.290	-64.0	...	4.0
36604.564 ..	0.298	-14.0	...	49.7
36605.476 ..	0.392	12.0	...	20.6
36613.497 ..	0.224	-65.0	...	38.5
36624.547 ..	0.369	-4.0	...	17.8
38844.402 ..	0.487	-9.0	...	-50.6
38858.343 ..	0.933	17.0	...	29.3
39180.472 ..	0.326	2.0	...	49.4
39180.578 ..	0.337	26.0	...	66.9
39186.428 ..	0.943	25.0	...	47.6
39186.521 ..	0.953	-11.0	...	21.0
39207.351 ..	0.112	-121.0	...	10.2
39207.465 ..	0.124	-114.0	...	17.5
39252.231 ..	0.764	56.0	...	-39.8
39269.208 ..	0.524	-8.0	...	-66.3
39518.485 ..	0.365	-24.0	...	0.2
39518.578 ..	0.375	-14.0	...	4.6
39556.424 ..	0.298	-58.0	...	5.5
39610.306 ..	0.884	-5.0	...	-37.3
39625.397 ..	0.448	-10.0	...	-32.0
39655.205 ..	0.538	38.0	...	-26.0
39655.304 ..	0.548	48.0	...	-20.1
40696.285 ..	0.460	16.0	...	-12.2
40696.492 ..	0.482	6.0	...	-32.8
40697.295 ..	0.565	21.0	...	-53.3
40697.469 ..	0.583	51.0	...	-29.5
40698.295 ..	0.669	101.0	...	0.9
40698.469 ..	0.687	101.0	...	-0.8
42119.780 ^b ..	0.025	-71.3	3.9	25.1	22
44258.512 ^c ..	0.734	121.4	...	20.4	1	-136.1	...	43.3	1
48676.621 ..	0.731	157.0	...	55.7	1	-124.0	...	55.9	1
48678.679 ..	0.944	38.0	...	61.4	1
48679.666 ..	0.046	-100.0	...	10.3	1	120.0	...	-81.2	1
48763.596 ..	0.747	61.0	...	-38.3	4	-122.0	...	54.3	4

Table 1—Continued

HJD (-2,400,000)	Orbital Phase	V_1 (km s ⁻¹)	σ_1 (km s ⁻¹)	$(O - C)_1$ (km s ⁻¹)	n_1	V_2 (km s ⁻¹)	σ_2 (km s ⁻¹)	$(O - C)_2$ (km s ⁻¹)	n_2
49028.717 ..	0.230	-118.0	...	-17.5	4	196.0	...	12.5	4
49151.548 ..	0.963	-2.0	...	40.3	2
49451.763 ..	0.085	-81.0	...	45.6	1	206.0	...	-24.5	1
49454.570 ..	0.376	-56.0	...	-37.8	1
50526.791 ..	0.526	68.4	3.6	9.5	15	-148.3	5.2	-44.7	15
50527.749 ..	0.625	92.9	0.9	0.6	11	-150.6	4.0	13.3	15
50528.796 ..	0.734	118.9	1.4	17.9	14	-188.7	4.5	-9.3	13
50529.763 ..	0.834	78.0	3.5	10.4	15	-110.6	9.4	8.7	12
50530.747 ..	0.936	-40.5	8.2	-25.0	14	23.8	22.3	-6.7	15
50531.724 ..	0.037	-109.2	5.3	-4.3	15	158.2	12.0	-33.1	12
50532.753 ..	0.144	-132.7	4.5	-2.8	13	215.0	7.0	-21.5	13
50533.724 ..	0.245	-77.2	3.1	16.0	14	149.0	3.6	-21.4	12
50534.758 ..	0.352	-46.5	7.4	-14.4	15	64.9	11.0	4.5	11
50535.737 ..	0.453	6.0	4.9	-18.5	15	14.7	10.7	56.4	15
50909.952 ..	0.246	-98.1	2.7	-5.5	7	193.8	7.0	24.4	7
50910.190 ..	0.270	-88.7	1.8	-9.4	7	168.5	2.1	23.1	6
50910.935 ..	0.348	-26.1	6.3	8.4	7	40.7	22.8	-24.0	7
50911.038 ..	0.358	-16.5	6.8	11.8	7	25.3	19.9	-28.1	7
50914.179 ..	0.684	112.6	2.8	11.0	7	-188.1	5.7	-7.6	7
50914.952 ..	0.764	97.7	1.0	1.8	6	-165.5	9.0	4.7	7
50916.148 ..	0.888	-0.4	9.5	-29.2	7
50916.913 ..	0.967	-28.8	4.6	17.5	7	98.2	5.6	12.3	6
50917.060 ..	0.983	-48.3	1.3	12.5	6	102.2	3.7	-9.9	6
50917.204 ..	0.997	-68.8	1.2	5.5	6	125.4	1.8	-11.1	6
50917.936 ..	0.073	-136.9	2.2	-13.9	7	252.4	9.7	28.4	7
50918.058 ..	0.086	-140.1	1.8	-13.2	7	253.4	8.5	22.2	7
50918.217 ..	0.102	-136.4	2.5	-6.2	7	255.5	9.4	18.4	7

^aFeast et al. (1955)

^bConti et al. (1977)

^cStickland & Lloyd (2001)

Table 2. Orbital Elements

Element	Value
P (days)	9.64659 (12)
T (HJD-2,400,000)	48650.28 (29)
e	0.156 (29)
ω ($^\circ$)	122 (12)
K_1 (km s $^{-1}$)	117 (4)
K_2 (km s $^{-1}$)	211 (7)
$V_{0\ 1}$ (km s $^{-1}$)	−4.9 (25)
$V_{0\ 2}$ (km s $^{-1}$)	11 (5)
$M_1 \sin^3 i$ (M_\odot).....	21.8 (21)
$M_2 \sin^3 i$ (M_\odot).....	12.1 (13)
$a_1 \sin i$ (R_\odot)	22.0 (7)
$a_2 \sin i$ (R_\odot)	39.7 (12)
r.m.s. $_1$ (km s $^{-1}$) ..	20.6
r.m.s. $_2$ (km s $^{-1}$) ..	25.4

Note. — Numbers in parentheses give the error in the last digit quoted.

Table 3. Stellar Properties

Property	Primary	Secondary
Spectral Classification	O6.5 V((f))	O8.5 V
Relative flux $F/F_1(4300\text{\AA})$..	1.0	0.54 ± 0.08
$V \sin i$ (km s^{-1})	102 ± 10	164 ± 12
T_{eff} (kK)	40.5 ± 1.5	35.0 ± 1.5
$\log L/L_{\odot}$	5.34 ± 0.08	4.91 ± 0.09
R/R_{\odot}	9.5 ± 0.9	7.7 ± 0.8
$(R_{\text{Roche}} \sin i)/R_{\odot}$ (periastron)	22.4 ± 1.0	17.1 ± 0.7
M/M_{\odot} (predicted)	36.2 ± 2.0	22.9 ± 1.1
M/M_{\odot} (observed limit)	$> 25.3 \pm 2.5$	$> 14.1 \pm 1.5$

Fig. 1.— The radial velocity measurements (*filled circles*: CASLEO and MSO data for the primary; *plus signs*: low weight data for the primary; *open circles*: CASLEO and MSO data for the secondary; *X signs*: low weight data for the secondary) and orbital solution (*solid lines*) plotted against orbital phase. Phase zero corresponds to the time of periastron.

Fig. 2.— Comparisons of the reconstructed primary spectra (MSO offset to a continuum of 2.8; CASLEO offset to a continuum of 2.5) and reconstructed secondary spectra (MSO offset to a continuum of 1.3; CASLEO at the normal continuum of 1.0) with spectra of the same classifications from Walborn & Fitzpatrick (1990). All the spectra were Gaussian smoothed to a nominal resolution of 1.2 Å FWHM for comparable line broadening.

Fig. 3.— H-R diagram for the components of HD 101131 (*filled circle*: primary; *open circle*: secondary). *Solid lines*: single star evolutionary tracks of Schaller et al. (1992) labelled by the initial stellar mass (M_{\odot}). *Diagonal error lines*: range in effective temperature and bolometric correction associated with the spectral classification. *Vertical error bars*: net error in luminosity for the adopted temperature. Our derived lower limits on the masses (25 and $14M_{\odot}$ for the primary and secondary, respectively) are consistent with the predicted evolutionary masses.

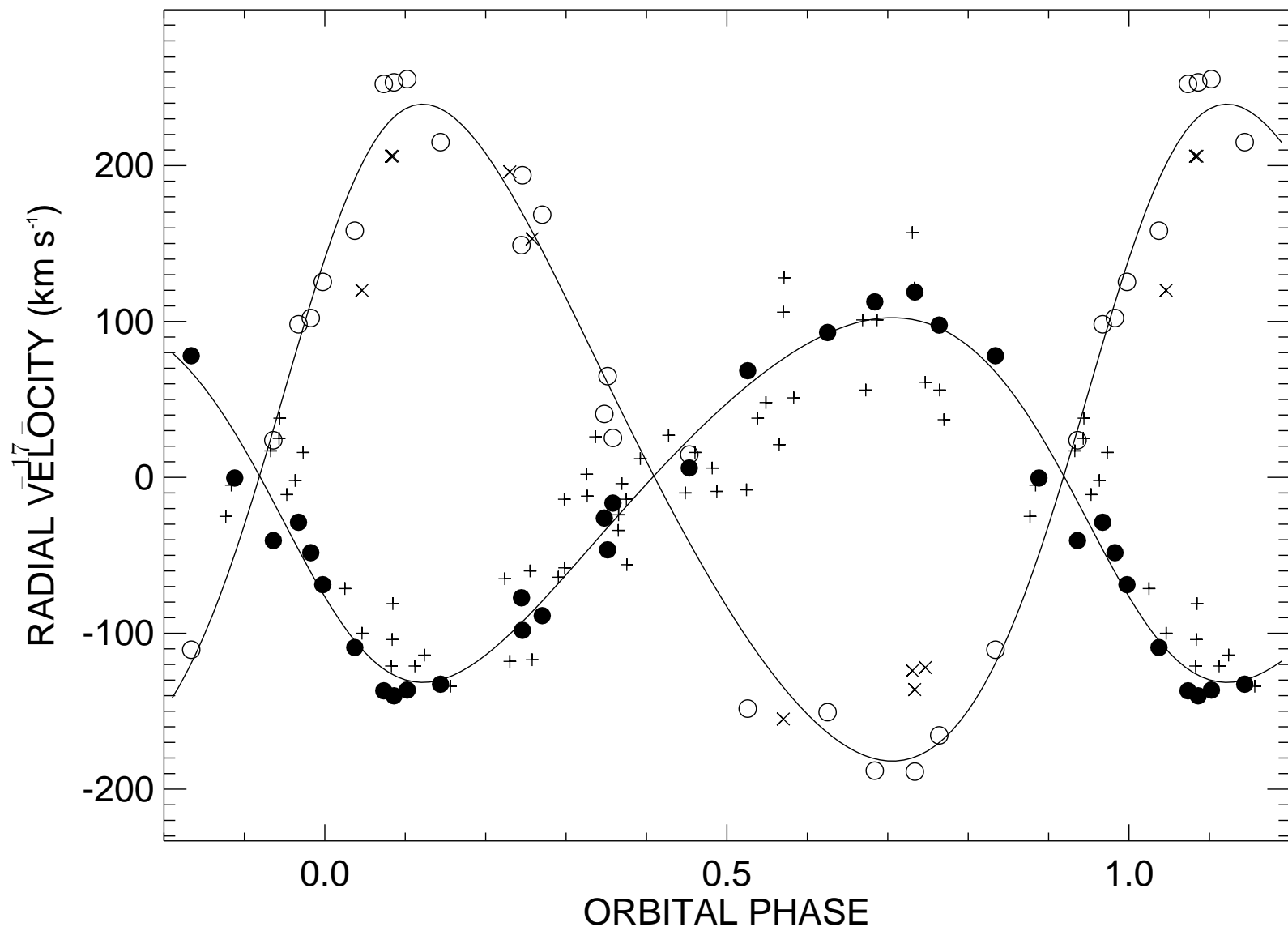


Fig. 1.—

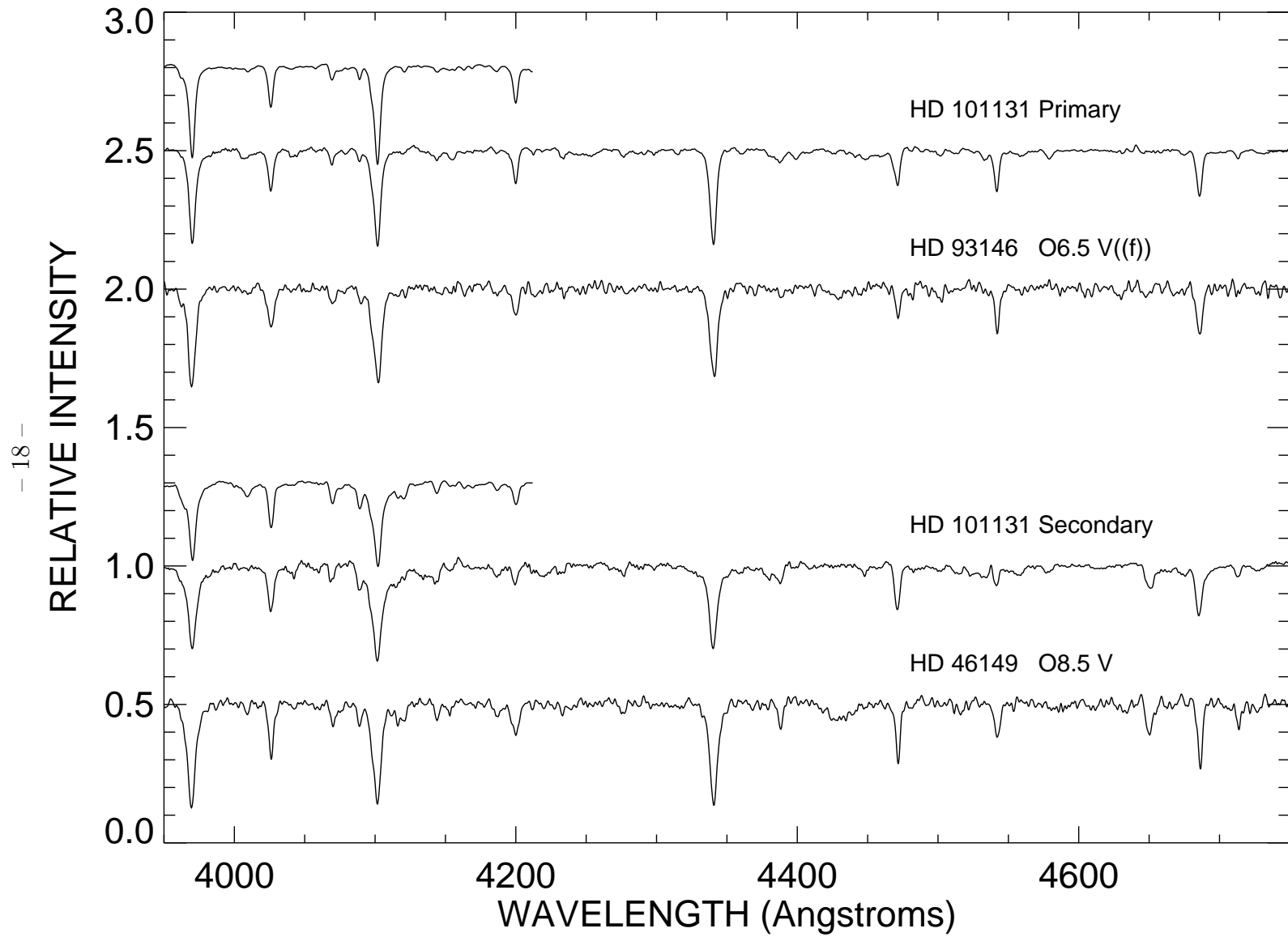


Fig. 2.—

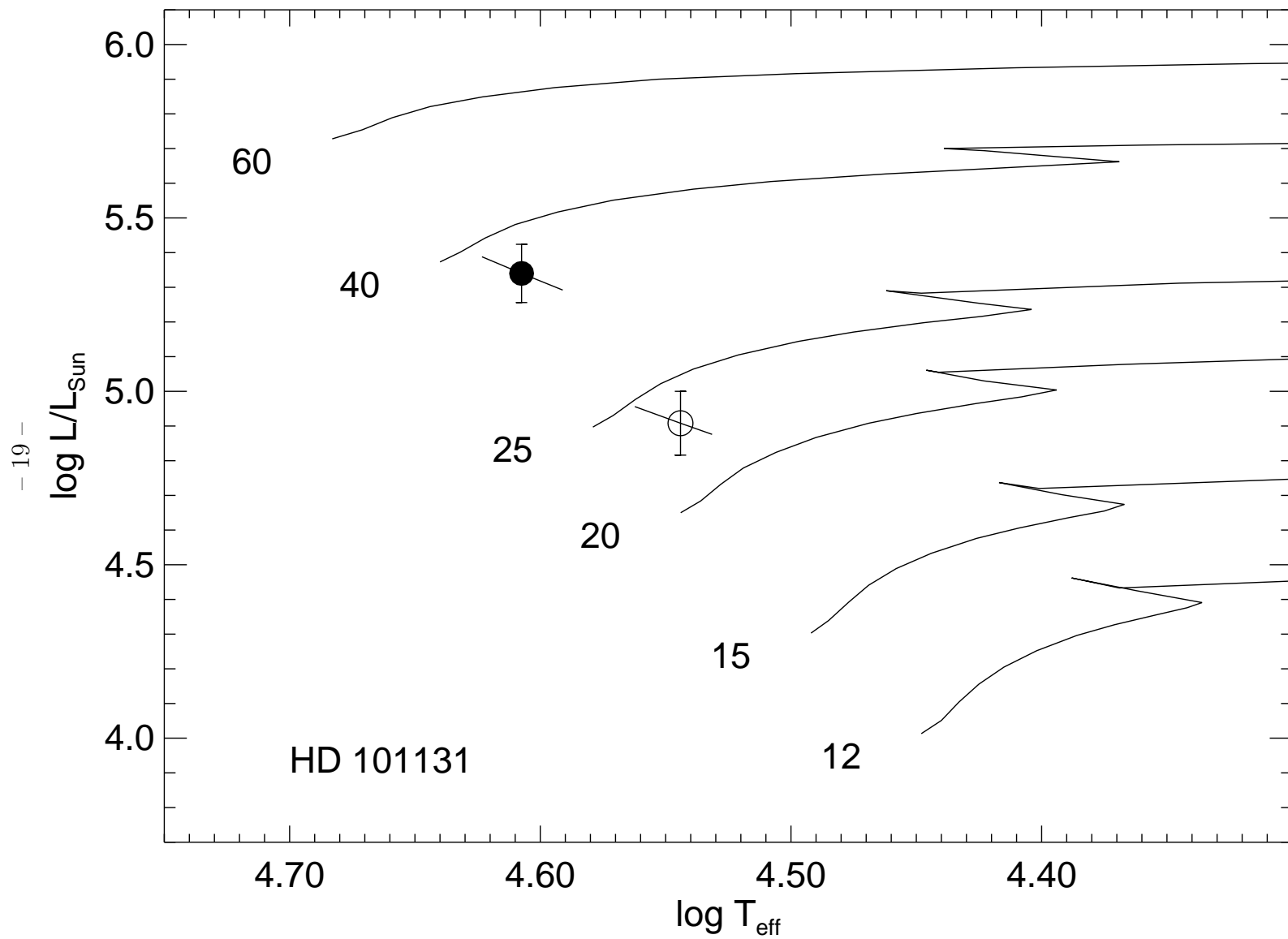


Fig. 3.—